Acta Crystallographica Section D
Biological Crystallography
ISSN 0907-4449

Structure-based enzyme inhibitor design: modeling studies and crystal structure analysis of *Pneumocystis carinii* dihydrofolate reductase ternary complex with PT653 and NADPH

Vivian Cody,[a]* Nikolai Galitsky,[a] Joseph R. Luft,[a] Walter Pangborn,[a] Andre Rosowsky[b] and Sherry F. Queener[c]

[a]Hauptman–Woodward Medical Research Institute, Inc., 73 High Street, Buffalo, NY 14203, USA, [b]Dana Farber Cancer Institute and Department of Biological Chemistry and Molecular Pharmacology, Harvard Medical School, 44 Binney Street, Boston, MA 02215, USA, and [c]Department of Pharmacology and Toxicology, Indiana University School of Medicine, Indianapolis, IN 46202, USA

Correspondence e-mail: cody@hwi.buffalo.edu

Received 10 December 2001
Accepted 18 March 2002

PDB Reference: NADPH–PT653–pcDHFR, 1klk, r1klksf.

Structural data are reported for *N*-(2,4-diaminopteridin-6-yl)methyldibenz[*b*,*f*]azepine (PT653), an example of structure-based inhibitor design with 21-fold selectivity for *Pneumocystis carinii* dihydrofolate reductase (pcDHFR) relative to rat liver dihydrofolate reductase (rlDHFR). These data test the hypothesis that 2,4-diaminopteridines with a bulky *N*,*N*-diarylaminomethyl side chain at the 6-position could fit better into the larger active site of pcDHFR than into that of mammalian DHFR. The crystal structure of the ternary complex of NADPH, PT653 and pcDHFR, refined to 2.4 Å resolution, reveals that PT653 binds in a different orientation than predicted from modeling studies reported previously [Rosowsky *et al.* (1999), *J. Med. Chem.* **42**, 4853–4860]. These crystal data show that the pteridine-ring plane is tilted compared with that observed in the crystal structure of the pcDHFR methotrexate (MTX) NADPH ternary complex used as a template to model PT653 binding. Also, as a result of this tilt, the dibenzoazepine ring is bound deeper into the *p*-aminobenzoyl folate binding pocket of pcDHFR, thereby relieving close intermolecular contacts predicted from the modeling data. By far the most significant structural change, but more subtle in magnitude, is the ligand-induced conformational shift of 1.2 Å away from the inhibitor of residues 61–66 in helix *C*. The other major effect is the unwinding of the short helical segment involving loop 47 which has a different conformation to that observed in other pcDHFR complexes [Cody *et al.* (1999), *Biochemistry*, **38**, 4303–4312]. The favorable pcDHFR selectivity of PT653 could be a result of ligand-induced fit of the large hydrophobic dibenzazepine ring which occupies regions of the enzyme active site not probed by other antifolates and which take advantage of sequence and conformational differences between the structures of human and pcDHFR. These data suggest that such hydrophobic analogs could be used as lead compounds in the design of more pcDHFR-selective antifolates. Enzyme inhibition data also show that PT653 is 102-fold selective for *Toxoplasma gondii* (tg) DHFR relative to rlDHFR. Homology-modeling studies of the tgDHFR structure suggest that differences in ligand-binding orientation and enzyme sequence could influence the enhanced selectivity of PT653 for tgDHFR.

1. Introduction

Pneumonia caused by opportunistic infectious agents is still a major cause of mortality among patients with AIDS or other forms of immunosuppression (Falloon & Masur, 1992; Klepser & Klepser, 1997; Kovacs *et al.*, 1984; Lundgren, 1994; Luft & Remington, 1992; Sattler *et al.*, 1994; Beaman *et al.*, 1992). Antifolates such as trimethoprim (TMP) have been shown to

be effective against the dihydrofolate reductase (DHFR) from *Pneumocystis carinii* (pc) and *Toxoplasma gondii* (tg). However, these antifolates have limited efficacy against pc and other parasitic organisms and there is a need for more effective inhibitors. Since immunosuppressed patients and those with AIDS are severely affected by these opportunistic pathogens, efforts have been focused on the design of antifolates that are selective against pcDHFR or tgDHFR (Broughton & Queener, 1991; Queener, 1991, 1995; Robson *et al.*, 1997; Jones *et al.*, 1999; Piper *et al.*, 1996; Gangjee, Elzein *et al.*, 1998; Gangjee *et al.*, 1999; Rosowsky *et al.*, 1997, 1998; Rosowsky, Papoulis *et al.*, 1999; Gangjee, Zhu *et al.*, 1998; Gangjee, Mavandadi *et al.*, 1997; Gangjee, Shi *et al.*, 1997; Then *et al.*, 1993).

Structural data for mammalian and pcDHFR inhibitor complexes have been carried out for a number of antifolates including TMP (Matthews *et al.*, 1985; Champness *et al.*, 1994), MTX and folate (FA; Kraut & Matthews, 1987; Cody *et al.*, 1992, 1993), as well as novel furopyrimidine classical and nonclassical antifolates (Cody *et al.*, 1997, 1998; Gangjee, Guo *et al.*, 1998; Gangjee, Vidwans *et al.*, 1998). These data show that key structural features of the active site are highly conserved, although there are a number of species-dependent residue changes within the active site of the DHFR. Thus, there is in pcDHFR a change from the human sequence of Phe31 to Ile33, Gln35 to Lys37 and Asn64 to Phe69. Comparison of these structures reiterates the role of selective inhibitor interactions with these mutational sites as a determinant of selectivity between human and pcDHFR. These data also show that the volume of the active site is slightly larger in the pcDHFR enzyme than in the human enzyme and that these small changes can enhance binding affinity and thus inhibitor selectivity for one enzyme over the other.

Structure-based design methods have also been used to analyze differences in the active-site regions of human and pcDHFR so as to better understand the structural features of these enzymes which control binding and selectivity. These studies have shown that novel compounds from diverse chemical classes can inhibit pcDHFR (Gschwend *et al.*, 1996, 1997; Farber, 1999). Similar studies comparing structural data for inhibitor complexes of human and pcDHFR have led to the design of a series of pteridine analogs that contain a large hydrophobic diarylamine side chain (Rosowsky, Cody *et al.*, 1999; Rosowsky *et al.*, 2000). These data test the hypothesis that 2,4-diaminopteridines with a bulky *N,N*-diarylaminomethyl side chain at the 6-position might fit better into the larger active site of pcDHFR than into that of mammalian DHFR. Among several analogs of this type that have been synthesized and tested (Rosowsky, Cody *et al.*, 1999; Rosowsky *et al.*, 2000) (Fig. 1), PT653 was the most selective, with an IC_{50}(rl)/IC_{50}(pc) of 21 compared with 0.07 for trimetrexate and 11 for TMP. These data suggest that PT653 could be a lead compound for structure-activity optimization. However, bioactivity data for analogs of PT653 in which the pteridine was modified to quinazoline and in which the C9–N10 bridge was reversed resulted in less selective but more potent analogs (Rosowsky *et al.*, 2000).

Structural data are reported for *N*-(2,4-diaminopteridin-6-yl)methyldibenz[*b*,*f*]azepine (PT653), an example of structure-based inhibitor design with 21-fold increased selectivity for *P. carinii* (pc) DHFR than for rlDHFR. These crystal structure results are compared with molecular-modeling data carried out on this series of antifolates (Rosowsky, Cody *et al.*, 1999; Rosowsky *et al.*, 2000). A model for tgDHFR has also been made using sequence-alignment profiles and the crystal structures of *Escherichia coli* and *Mycobacterium tuberculosis* DHFR to rationalize the 102-fold selectivity of PT653 for tgDHFR.

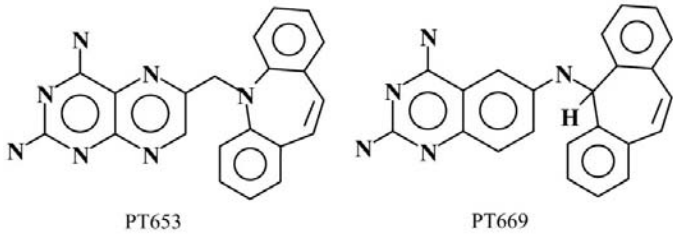

Figure 1
Schematic representation of PT653 and PT669.

2. Experimental section

2.1. Crystallization and X-ray data collection

Recombinant pcDHFR was purified as described previously (Broughton & Queener, 1991). A buffer exchange was carried out in a Centricon 10 ultrafiltration cell with 100 m*M* KCl, 50 m*M* MES buffer pH 6.0. The protein solution was incubated for 18 h with NADPH and PT653 at 277 K, after which it was concentrated to 6 mg ml^{-1}. Crystallization experiments were conducted using a capillary microbatch method (Luft *et al.*, 1999*a*) set up on a polythermal gradient (Luft *et al.*, 1999*b*). Crystals were grown in a 0.7 mm diameter special glass X-ray capillary that contained 3 mg ml^{-1} protein solution, 20%(*w*/*v*) PEG 2000 MME, 100 m*M* KCl, 50 m*M* MES buffer pH 6.0.

Data collection was carried out at room temperature to 2.4 Å resolution using a Rigaku R-AXIS IV imaging-plate system with a rotating-anode source. Diffraction data showed a monoclinic lattice, space group $P2_1$, with unit-cell parameters a = 36.836, b = 43.138, c = 59.319 Å, β = 95.03° for the ternary complex. Data were processed with the *HKL* package (Otwinowski & Minor, 1997). Crystal lattice properties and data-collection statistics are listed in Table 1.

2.2. Structure determination and refinement

The initial structure of the pcDHFR–NADPH–PT653 complex was solved by molecular-replacement methods using the protein coordinates from the ternary complex of the furopyrimidine pcDHFR complex (Cody *et al.*, 1997), minus the cofactor and inhibitor atoms, with the program *CNS* (Brünger *et al.*, 1998) in combination with the model-building program *CHAIN* (Sack, 1988). A total of 10% of the reflections were randomly selected prior to the refinement to calculate R_{free} values for cross validation (Brünger, 1992;

Table 1
Crystal properties and refinement statistics for pcDHFR–PT653–NADPH complex.

Space group	$P2_1$
Unit-cell parameters (Å, °)	a = 36.836, b = 43.138, c = 59.319, β = 95.03
Resolution range (Å)	8.0–2.4
Reflections used	5802
Reflections, R_{free}	634
R factor (%)	19.6
R_{free} (%)	28.9
Protein atoms	1661
Water molecules	33
B factor (protein average) (Å^2)	44.4
R_{merge} (%)	7.3
Completeness (2.49–2.40 Å) (%)	89.5
R.m.s.d. bond lengths (Å)	0.008
R.m.s.d. bond angles (°)	1.52

Adams *et al.*, 1997). The model was refined by iterative cycles of B-factor and positional refinement followed by simulated annealing with slow-cooling protocols. The initial $(2|F_o| - |F_c|)\exp(i\alpha_c)$ maps, where F_o are the observed and F_c the calculated structure factors based on the protein model only and α_c is the calculated phase, resulted in electron density corresponding to both the inhibitor PT653 and the cofactor NADPH (Fig. 2), as well as a good fit of the protein to its density. Between least-squares minimizations, the structure was manually adjusted to fit difference electron density and verified by a series of omit maps calculated from the current model with deleted fragments. The final refinement statistics are summarized in Table 1. The Ramachandran conformational parameters from the last cycle of refinement generated by *PROCHECK* (Laskowski *et al.*, 1993) show that more than 87% of the residues have the most favored conformation and none are in disallowed regions. Coordinates for this structure have been deposited with the Protein Data Bank.

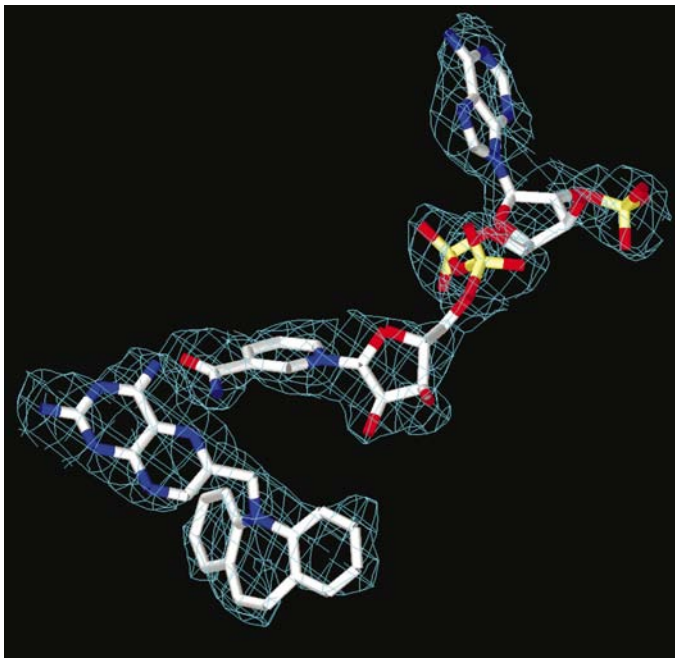

Figure 2
View of the electron density ($2F_o - F_c$, 1σ) (blue) showing the fit of the inhibitor PT653 and NADPH shown with atom type colors. Model produced using *SETOR* (Evans, 1993).

Table 2
Active-site residues in various DHFR species.

Residue species†	23	24	25	32	33	34	36	37	69	75
Human	Gly	Asp	Leu	Glu	Phe	Tyr	Phe	Gln	Asn	Arg
Rat‡	Gly	Asp	Leu	Glu	Phe	Tyr	Phe	Gln	Asn	Arg
pc	Gln	Ser	Leu	Glu	Ile	Tyr	Phe	Lys	Phe	Arg
ec	Asn	Ala	Met	Asp	Leu	Tyr	Phe	Lys	Arg	Arg
mtb	Gly	Asp	Ile	Asp	Glu	His	Phe	Arg	Val	Arg
tg	Glu	Glu	Leu	Asp	Phe	His	Phe	Ser	Phe	Arg

† Numbering from pcDHFR sequence. ‡ Wang *et al.* (2001).

2.3. Modeling studies

PT653 and its analogs (Fig. 1) were generated using the *SYBYL* (Tripos Inc.) builder function followed by energy minimization of the resulting structure. A search of the Cambridge Structural Database did not reveal suitable candidates for the seven-membered ring structure. In the case of the seven-membered ring structure, more than one conformer is accessible depending on the pucker of the seven-membered ring. In addition, inversion of the pyramidal nitrogen at N10 results in non-superimposable conformers, as do the racemates of the reverse N9–C10 bridge analogs.

In earlier studies, the pteridine ring of tested analogs was mapped to the pteridine ring of methotrexate (Rosowsky, Cody *et al.*, 1999). In this case, the preliminary fit of the reverse-bridge quinazolines (Rosowsky *et al.*, 2000) was made by superimposition on that of PT653, as observed in its crystal structure. The models were then adjusted manually to optimize fit. Intermolecular contacts were measured between the analog dibenzazepine-ring positions and their nearest neighbors in the active site, similar to the protocol carried out for the previous modeling study (Rosowsky, Cody *et al.*, 1999).

A model of the tgDHFR active site was made based on the sequence alignment of tgDHFR (Roos, 1993) and the crystal structures of *E. coli* (ec) DHFR MTX complexes (Matthews *et al.*, 1985; Kraut & Matthews, 1987) and *M. tuberculosis* (mtb) DHFR TMP ternary complex (Li *et al.*, 2000). Like the bacterial enzymes including mtbDHFR, tgDHFR also has an Asp for Glu32 substitution as its acidic residue in the active site (Table 2). Other similarities between the sequence of tgDHFR and mtbDHFR are a substitution of His for Tyr in position 34. Like pcDHFR, there is a Phe for Asn substitution in position 69, whereas there is a Val at this position in mtbDHFR. Among the bacterial forms of the enzyme, ecDHFR and mtbDHFR have a closer degree of similarity to tgDHFR than pcDHFR and thus were both used as a templates for tgDHFR.

3. Results and discussion

3.1. Overall structure

Although the structure of the pcDHFR PT653 ternary complex (Fig. 3) is similar to that of other antifolate–DHFR complexes, significant changes in the protein conformation are observed in flexible loop regions. The major conformational difference between PT653 and FA or MTX pcDHFR ternary complexes involve loop 47 (residues 45–50; Cody *et al.*, 1999). In most pcDHFR structures, loop 47 forms a short helical turn. In the PT653 structure, the loop has unwound, exposing Phe46 and Phe49 to the enzyme surface. This change was originally observed in the structure of the binary FA pcDHFR complex (Cody *et al.*, 1999). However, superposition of the structures of the MTX, FA and PT653 complexes reveals that the loop 47 conformation differs in each of the structures (Fig. 4). The PT653 complex represents another point along a series of conformational changes for unfolding the short helical turn in loop 47.

Previous analysis of the FA and MTX pcDHFR complexes had suggested that packing interactions present in the orthorhombic FA binary complex lattice, compared with the monoclinic MTX ternary lattice, stabilized the conformational changes in loop 47 by formation of a series of tight hydrogen bonds to the carbonyl O atoms of both Phe46 and Phe49 and the amine of Lys73 (Cody *et al.*, 1999). Despite the fact that the structure of the PT653 ternary complex is isomorphous to the monoclinic lattice of the MTX pcDHFR complex, the intermolecular interactions of loop 47 in this structure more closely resemble those for the orthorhombic FA complex (Cody *et al.*, 1999) (Table 3; Figs. 4 and 5). In this monoclinic packing arrangement, Lys31 from a symmetry-related enzyme forms a series of hydrogen bonds with the backbone carbonyl and amide of Phe46 and Asp47 (Table 3). In this conformation,

Table 3
Hydrogen-bond interactions (Å) of loop 47 in the pcDHFR–PT653 complex.

* refers to a symmetry-related molecule in the crystal lattice.

Monoclinic lattice with extended turn conformation (PT653 complex)	
Phe46 O···N Gln68*	2.8
Phe49 N···NZ Lys31*	2.6
Asp47 O···NZ Lys31*	3.0
Asp47 N···O Thr45	3.2
Asp47 OD2···N Gln118	2.9
Orthorhombic lattice with loop 47 in extended conformation (FA complex†)	
Phe46 O···NZ Lys73*	2.6
Ser48 O^{γ}···NH1 Arg70*	3.1
Phe49 O···NZ Lys73*	2.7
Asp47 OD1···N Gln68*	2.9
Glu50 OE2···NZ Lys73*	2.9
Asp47 OD2···Wat	2.9
Monoclinic lattice with short helical turn conformation (MTX complex†)	
Phe46 O···N Ser48	2.7
Phe49 N···N Ser48	2.9
Ser48 O^{γ}···O Pro44	3.0
Glu50 OE1···NZ Lys31*	3.0

† Cody *et al.* (1999).

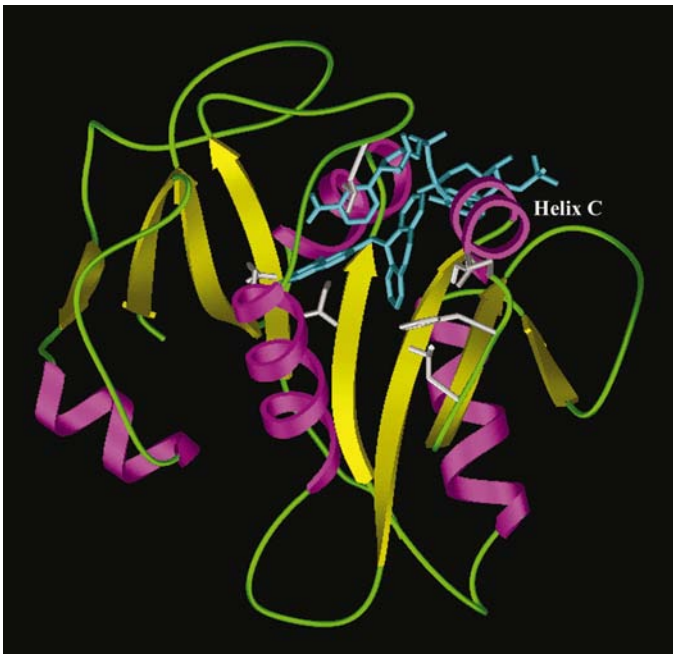

Figure 3
Tertiary crystal structure of pcDHFR–PT653–NADPH ternary complex. Helices are violet, sheets are yellow and loops are green. Helix *C* encompasses residues 61–66. The inhibitor and cofactor are cyan and key active-site residues are white. Model produced using *SETOR* (Evans, 1993).

Figure 4
Comparison of pcDHFR–PT653–NADPH ternary complex highlighting the conformation of loop 47 and the disposition of Phe46 and Phe49 (white) with that of pcDHFR–FA binary complex (green) and with pcDHFR–MTX–NADPH ternary complex (orange).

Ser48 does not participate in any intermolecular interactions as was observed in the MTX and FA complexes (Cody *et al.*, 1999).

3.2. Inhibitor binding

The positions of PT653 and NADPH were clearly defined in difference electron-density maps (Fig. 2). These structural data reveal that PT653 binds in a different orientation to that predicted from modeling studies (Rosowsky, Cody *et al.*, 1999) and to that observed in the MTX ternary pcDHFR complex (Cody *et al.*, 1999) (Fig. 6). The plane of the PT653 pteridine ring is tilted about 10° from that of MTX, thereby placing the dibenzazepine ring deeper in the *p*-aminobenzoyl ring pocket and relieving the short intermolecular contacts observed in the previously reported modeled structure (Rosowsky, Cody *et al.*, 1999). Despite the change in pteridine-ring orientation, the carboxylate O atoms OE2 and OE1 of Glu32 still maintain their hydrogen-bonding interactions to N(1) and the 2-amino group. In addition, the carboxylate O atoms of the glutamate form hydrogen bonds to a conserved Thr144 and to a conserved structural water. Further comparisons between the crystal structure and the modeling data suggest that, within the error of these structure determinations, the dibenzazepine ring is more planar than in the modeled structure, which again results in fewer close intermolecular contacts with the side-chain residues in helix *C* (residues 61–66).

Fig. 6 also highlights differences between the human and pcDHFR ternary complexes. Of interest is the observation that the backbone of helix *C* has shifted about 1.2 Å away from the inhibitor compared with other DHFR complexes (Table 4). Such ligand-induced conformational changes had also been noted in the structures of the FA binary and ternary structures (Cody *et al.*, 1999; Saway & Kraut, 1997). As illustrated (Table 4), the PT653 DHFR complex has the largest contact distance between the C^{α} atom of Glu32 and that of Ile65 in helix *C*. Changes in the orientation of the diamino ring of the inhibitors are also reflected in the variability of the contacts between the carboxylate O atom of the acidic function (Glu or Asp) and the helix *C* residue (Ile65).

3.3. NADPH binding

Although the NADPH is bound in an extended conformation similar to other cofactor complexes (Cody *et al.*, 1999), there is significant variation in the conformation of the nicotinamide-ribose and the pyrophosphate moieties (Table 5; Fig. 7) compared with those observed in the MTX or FA complexes reported previously (Cody *et al.*, 1999). This structure shows an unusual *cis–trans* configuration at the pyrophosphate bridge. These changes are a reflection of the interactions of the cofactor with helix *C*. The *cis* conformation of the invariant glycines (Gly124, Gly125) and the interactions with residues Gly125, Ala126 and Asn127 permits interaction with the pyrophosphate O atoms positioned at the end of central helix *C*.

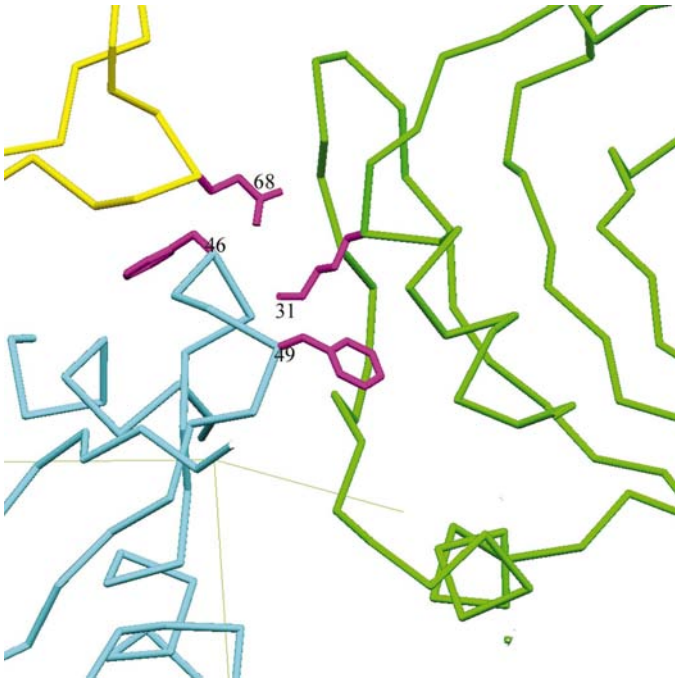

Figure 5
Packing environment of loop 47 in pcDHFR–PT653–NADPH (symmetry: x, y, z, cyan; $-x$, $y + 1/2$, $-z$; green, $x - 1$, y, z, yellow) showing the intermolecular interactions between Phe46 and Phe49 with Gln68 and Lys31 (violet) from neighboring molecules. Thin green lines are the outline of the unit cell.

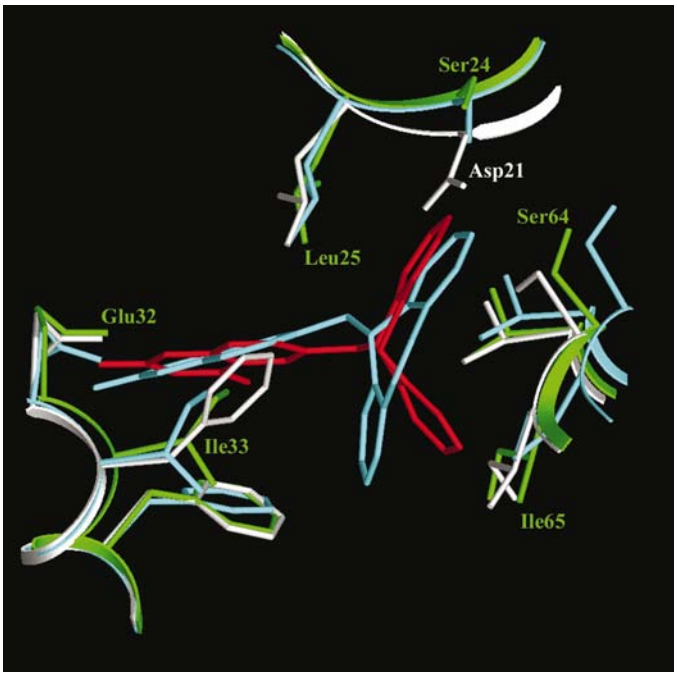

Figure 6
Comparison of the binding of PT653 modeled (red) into the active site of human (white) and pcDHFR (green) and that observed from its crystal structure determination (cyan). The largest difference is in the orientation of the pteridine ring compared with that modeled in the pteridine-ring position observed for methotrexate.

Table 4
Active-site dimensions in DHFR complexes.

Species	Residue†	Residue	Contact (Å)
pc PT653	Glu32 C^{α}	Ile65 C^{α}	15.9
	Glu32 OE1	Ile65 C^{α}	13.7
pc MTX	Glu32 C^{α}	Ile65 C^{α}	14.7
	Glu32 OE1	Ile65 C^{α}	12.7
Human MTX	Glu30 C^{α}	Ile60 C^{α}	14.6
	Glu30 OE1	Ile60 C^{α}	12.6
mtb TMP	Asp27 C^{α}	Leu50 C^{α}	14.7
mtb TMP	Asp27 OE1	Leu50 C^{α}	11.9
ec MTX	Asp27 C^{α}	Ile50 C^{α}	14.4
	Asp27 OE1	Ile50 C^{α}	12.3

† Structurally equivalent residues in each of the DHFR species.

Table 5
Cofactor conformation in pcDHFR ternary complexes.

NADPH/ $NADP^+$	Torsion angle†	PT653, $P2_1$	MTX‡, $P2_1$	FA‡, $P2_1$
χ_n	C5—N1—C6—C7	111.6	128.2	119.3
ξ_n	C8—C9—C10—O4	−142.8	−168.3	−178.4
θ_n	C9—C10—O4—P_n	−127.2	165.7	123.7
ψ_n	C10—O4—P_n—O7	−2.2	59.3	67.3
φ_n	O4—P_n—O7—P_a	176.6	105.9	58.9
φ_a	Pn—O7—P_a—O8	85.9	118.6	176.4
ψ_a	O7—P_a—O8—C11	−93.5	−77.6	−61.5
θ_a	P_a—O8—C11—C12	−173.4	−152.8	−149.5
ξ_a	O8—C11—C12—C13	−131.8	−170.9	164.6
χ_a	C14—C15—N2—C20	82.8	−122.7	−114.8
θ'_a	C15—C14—O10—P3	−164.3	163.4	162.8

† Subscript *n*, torsion angles for nicotinamide nucleoside; subscript *a*, torsion angles for adenine nucleoside. ‡ Cody *et al.* (1999).

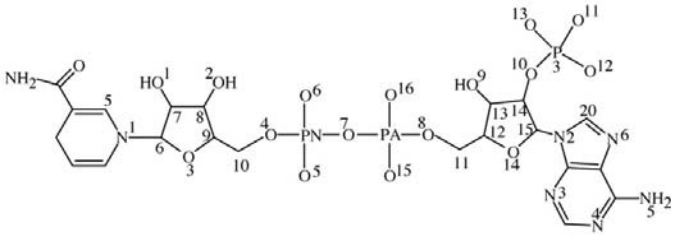

Figure 7
Atom numbering in NADPH/$NADP^+$ cofactor (see Table 5).

3.4. Molecular modeling

Numerous molecular-modeling studies have been carried out to aid in the identification of key enzyme residues that confer species selectivity on pcDHFR (Gschwend *et al.*, 1996, 1997; Farber, 1999; Cody *et al.*, 2000). Prior to the determination of this crystal structure, manual docking studies of PT653 and its analogs were carried out using the structural data for the ternary complex with MTX and NADPH (Rosowsky, Cody *et al.*, 1999). On the basis of this study, it was shown that the active site of the human DHFR (hDHFR) structure was more restricted than the pcDHFR site as indicated by the close contacts between the PT analog and the enzyme.

Comparison of a series of PT653 analogs that had either a quinazoline-ring substitution pattern or a reversed C9–N10 bridge showed that the potency of the reverse-bridge quinazoline, PT669 (Fig. 1), was similar to that of PT653 (IC_{50} 0.51 and 0.21 μ*M*, respectively), but that it was 230 times more potent against rlDHFR (IC_{50} 4.4 and 0.019 μ*M*, respectively). Despite its potency, PT669 has reverse selectivity (IC_{50} rl/pc 0.037; Rosowsky *et al.*, 2000).

The key elements that distinguish PT653 and PT669 are the differences in basicity between the pteridine-ring and quinazoline-ring structures and the fact that reversal of the N9–C10 bridge results in alternate bound stereoisomeric forms of PT669 that can map a different conformational space. There is also a loss of hydrogen bonding in the quinazoline structure, as N8 of the pteridine ring is known to make a hydrogen-bonding contact with a structural water in the active site of both hDHFR and pcDHFR.

Conformational modeling of PT669 indicates two bound isomers are possible because the seven-membered ring contains a tetrahedral sp^3 carbon at the bridgehead. Computer-modeling studies of PT669 racemates with pcDHFR–PT653–NADPH and hDHFR–MTX–NADPH ternary complexes (Fig. 8*a*) reveal that one bound isomer mirrors the intermolecular interactions of the orientation of bound PT653, while the other makes highly unfavorable contacts to the enzyme that are more severe in the human enzyme. In the unfavorable bound form of PT669, close contacts between the side chain of Leu25 and inhibitor range between 1.7 and 2.3 Å, well below the sum of the van der Waals radii for such hydrophobic contacts. In the hDHFR active site, this bound form of PT669 makes its closest contact (0.9 Å) with Phe31. In the more favorable form, the closest contacts are with Ser64 (2.7–2.9 Å) for both pcDHFR and hDHFR. Similarly, if PT669 is oriented in the MTX-bound position (Fig. 8*b*), there are more unfavorable contacts with Leu65 and Phe31. These data suggest that only one stereochemical orientation of PT669 is active and that the true selectivity of this analog is masked. Activity data for each stereochemical form is needed to determine whether further selectivity could be achieved using this as a lead compound.

3.5. Homology modeling

Conformational studies were also carried out with PT653 in the homology-modeled structure for tgDHFR. Sequence alignment of tg, pc, mtb, ec and hDHFR using *CLUSTAL* (Wisconsin Package, Version 10.0, Genetic Computing Program) reveal that the key active-site features are conserved and that the major differences among enzymes are substitution of Asp for Glu as the acidic residue in the active site (Table 2; Roos, 1993). Other changes in the active-site binding region are residues at pcDHFR Gln23 and Ser24 (Gly, Asp in hDHFR and Glu, Glu in tgDHFR). Since no structural data are available for tgDHFR, the crystal structures of ecDHFR (Matthews *et al.*, 1985) and of mtb DHFR as the TMP–NADPH ternary complex (Li et al., 2000) were used to model the changes involved with inhibitor binding to Asp.

Superposition of the pcDHFR PT653 complex on that of mtbDHFR structure shows that the primary effect of the Asp

for Glu substitution was in the orientation of the inhibitor (Fig. 9). In addition to the displacement of the pteridine ring because of the shorter Asp side chain, there is also a tilt in PT653 with respect to the position of TMP in the mtbDHFR structure. However, modeling PT653 in the TMP position causes the tricyclic ring to clash with the side chains of helix *C* and Leu31. Thus, it is likely that there will be a shift in ligand binding with tgDHFR. It is also likely that the loop region containing Leu25 and Ser24 (pcDHFR numbering) will change, as the substitution of Glu for Ser at position 24 of pcDHFR would produce different interactions with PT653. These data suggest that the enhanced selectivity of PT653 for tgDHFR over pcDHFR could be a consequence of the changes in sequence and conformation.

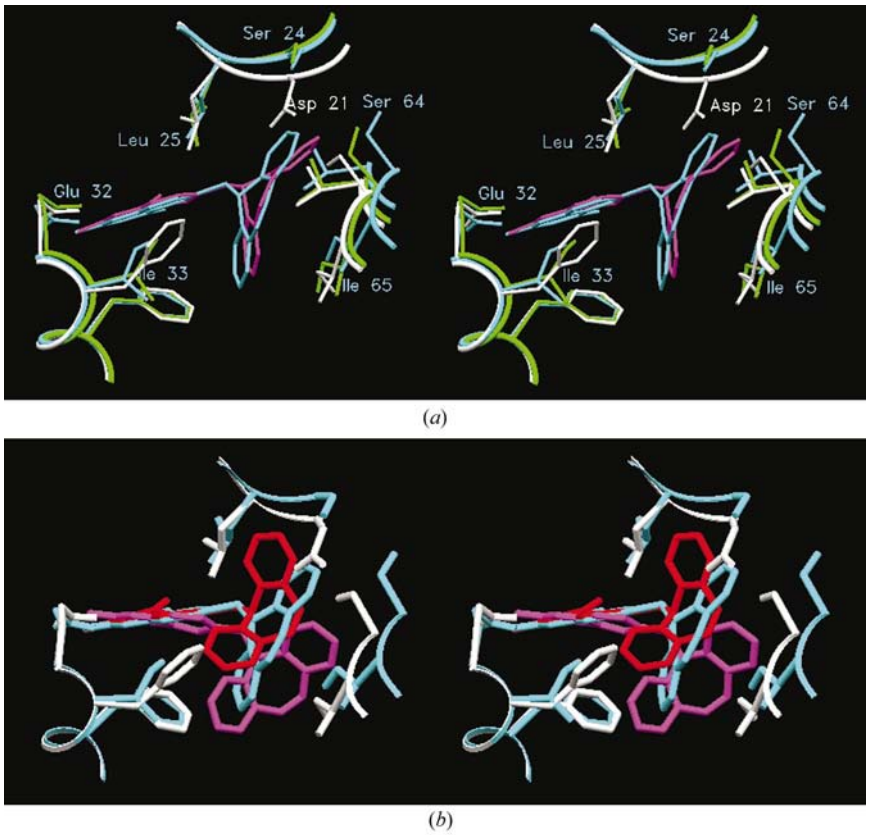

Figure 8
(*a*) Comparison of the binding of the reverse-bridge quinazoline, PT669 (violet) modeled in the active site of the crystal structures of hDHFR (white), pcDHFR MTX (green) (not shown) and pcDHFR PT653 (cyan). Only selected protein atoms are shown. (*b*) Comparison of the binding of PT669 (violet), bound in the orientation of MTX, the unfavorable stereo conformer of PT669 (red) and PT653 (cyan) in the active site of hDHFR (white) and the pcDHFR PT653 complex (cyan). Note the unfavorable contacts made by PT669 in the respective orientations.

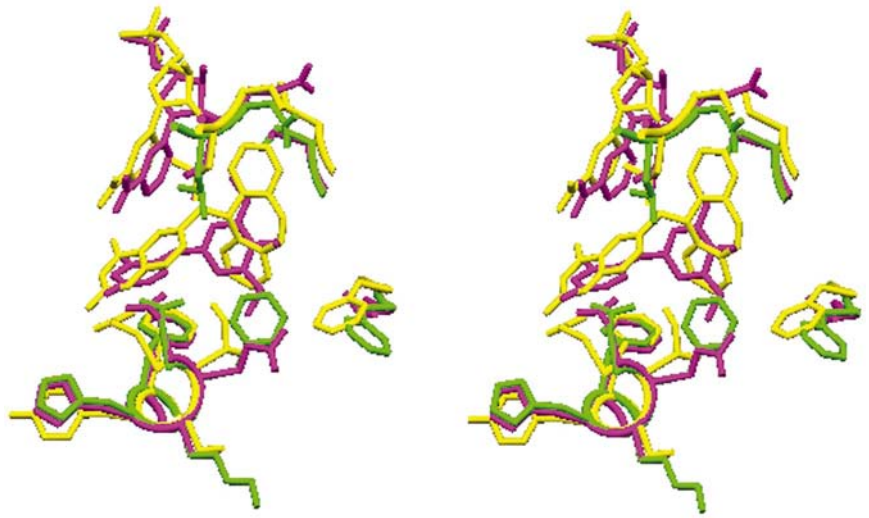

Figure 9
Comparison of the binding of PT653 (yellow) in the active site of the homology-modeled tgDHFR (green) and that of the mtbDHFR–TMP–NADPH (violet) complex.

4. Summary

These crystallographic studies describe structural comparisons of a structure-based designed ligand with other antifolate complexes and shows another example of ligand-induced conformational changes in pcDHFR, with large movements of the flexible loops encompassing residues 45–50 (loop 47). There was no evidence of movement of the flexible loop 23, as observed for the FA binary pcDHFR complex compared with the ternary complex. As a result of the conformational flexibility of this pcDHFR structure, subdomain movements were observed in this complex that differ from previously reported structures (Cody *et al.*, 1999).

These data further show that the orientation of the inhibitor differs significantly from that predicted from modeling studies. The major difference in binding orientation is a tilt of the pteridine-ring system with respect to that observed for classical antifolates such as MTX. Even though the hydrogen-bonding environment of the pteridine ring is maintained, the shift in orientation permits the bulky hydrophobic benzazepine-ring system to be better accommodated in the active site, thereby relieving many of the steric constraints present in the modeling data.

Previous studies (Rosowsky, Cody *et al.*, 1999) were carried out utilizing only manual modeling techniques rather than full molecular-dynamics simulations as was performed for the pcDHFR TAB complex (Cody *et al.*, 2000); therefore, these results did not address the effects of the change in torsion angle of the bound pteridine ring

compared with that of MTX. These studies also did not take into account the subdomain shifts that are possible in the absence of ligand in the *p*-aminobenzoyl pocket which permits hydrogen bonding between Lys37 and Arg75. Additionally, molecular-dynamics simulations of PT653 binding may not have predicted the ligand-induced conformational changes, particularly of the magnitude observed in this structure.

Homology modeling of the active site of tgDHFR, using the crystal data for ecDHFR (Matthews *et al.*, 1985) and mtbDHFR (Li *et al.*, 2000) as a template, reveals that the primary effect of the Asp for Glu substitution in the active site is to reorient the inhibitor with respect to the enzyme. This then places the inhibitor in a more favorable position to interact with the hydrophobic pocket of tgDHFR compared with pcDHFR. However, this simplistic model cannot predict the real structure of tgDHFR, but can provide a basis for further study of structure-based drug design. Therefore, antifolates such as PT653 can be used as targets for further structure-based design of new inhibitors of DHFR that can probe specific regions of the active site and confer greater specificity for either pcDHFR or tgDHFR.

We thank Dawn Rak for crystallization experiments. This work was supported in part by GM-51670 (VC), AI-29904 (AR) and NIH contract NO1-AI-35171 (SFQ).

References

Adams, P., Pannu, N., Read, R. & Brünger, A. (1997). *Proc. Natl Acad. Sci. USA*, **94**, 5018–5023.

Beaman, M. H., Luft, B. J. & Remington, J. S. (1992). *Ann. Intern. Med.* **117**, 163–164.

Broughton, M. C. & Queener, S. F. (1991). *Antimicrob. Agents Chemother.* **35**, 1348–1355.

Brünger, A. T. (1992). *Nature (London)*, **355**, 471–475.

Brünger, A. T., Adams, P. D., Clore, G. M., DeLano, W. L., Gros, P., Grosse-Kunstleve, R. W., Jiang, J.-S., Kuszewski, J., Nilges, M., Pannu, N. S., Read, R. J., Simonson, T. & Warren, G. L. (1998). *Acta Cryst.* D**54**, 905–921.

Champness, J. N., Achari, A., Ballantine, S. P., Bryant, P. K., Delves, C. J. & Stammers, D. K. (1994). *Structure*, **2**, 915–924.

Cody, V., Chan, D., Galitsky, N., Rak, D., Luft, J. R., Pangborn, W., Queener, S. F., Laughton, C. & Stevens, M. F. G. (2000). *Biochemistry*, **39**, 3556–3564.

Cody, V., Galitsky, N., Luft, J. R., Pangborn, W., Blakley, R. L. & Gangjee, A. (1998). *Anticancer Drug Des.* **13**, 307–315.

Cody, V., Galitsky, N., Luft, J. R., Pangborn, W., Gangjee, A., Devraj, R., Queener, S. F. & Blakley, R. L. (1997). *Acta Cryst.* D**53**, 638–649.

Cody, V., Galitsky, N., Rak, D., Luft, J. R., Pangborn, W. & Queener, S. F. (1999). *Biochemistry*, **38**, 4303–4312.

Cody, V., Luft, J. R., Ciszak, E., Kalman, T. I. & Freisheim, J. H. (1992). *Anticancer Drug Des.* **7**, 483–491.

Cody, V., Wojtczak, A., Kalman, T. I., Freisheim, J. H. & Blakley, R. L. (1993). *Chemistry and Biology of Pteridines and Folates*, edited by J. E. Ayling, M. G. Nair & C. M. Baugh, pp. 481–486. New York: Plenum Press.

Evans, S. V. (1993). *J. Mol. Graph.* **11**, 148–153.

Falloon, J. & Masur, H. (1992). In *Aids: Etiology, Diagnosis and Prevention*, 3rd ed., edited by V. T. DeVita, S. Hellman & S. A. Rosenberg. Philadelphia: Lippincott.

Farber, G. K. (1999). *Pharmacol. Ther.* **84**, 327–332.

Gangjee, A., Adair, O. & Queener, S. F. (1999). *J. Med. Chem.* **42**, 2447–2455.

Gangjee, A., Elzein, E., Queener, S. F. & McGuire, J. J. (1998). *J. Med. Chem.* **41**, 1409–1416.

Gangjee, A., Guo, X., Queener, S. F., Cody, V., Galitsky, N., Luft, J. R. & Pangborn, W. (1998). *J. Med. Chem.* **41**, 1263–1271.

Gangjee, A., Mavandadi, F. & Queener, S. F. (1997). *J. Med. Chem.* **40**, 1173–1177.

Gangjee, A., Shi, J. & Queener, S. F. (1997). *J. Med. Chem.* **40**, 1930–1936.

Gangjee, A., Vidwans, A. P., Vasudevan, A., Queener, S. F., Kisliuk, R. L., Cody, V., Li., R., Galitsky, N., Luft, J. R. & Pangborn, W. (1998). *J. Med. Chem.* **41**, 3426–3434.

Gangjee, A., Zhu, Y. & Queener, S. F. (1998). *J. Med. Chem.* **41**, 5433–5441.

Gschwend, D. A., Good, A. C. & Kuntz, I. D. (1996). *J. Mol. Recog.* **9**, 175–186.

Gschwend, D. A., Sirawaraporn, W., Santi, D. V. & Kuntz, I. D. (1997). *Proteins Struct. Funct. Genet.* **29**, 59–67.

Jones, M. L, Baccanari, D. P., Tansik, R. L., Boytos, C. M., Rudolph, S. K. & Kuyper, L. F. (1999). *J. Heterocycl. Chem.* **36**, 145–148.

Klepser, M. E. & Klepser, T. B. (1997). *Drugs*, **53**, 40–73.

Kovacs, J. A., Hiemenz, J. W., Macher, A. M., Stover, D., Murray, H. W., Shellhamer, J., Lane H. C., Urmacher, C., Honig, C., Longo, D. L., Parker, M. M., Natanson, C., Parrillo, J. E., Fauci, A. S., Pizzo, P. A. & Masur, H. (1984). *Ann. Intern. Med.* **100**, 663.

Kraut, J. & Matthews, D. A. (1987). *Biological Macromolecules and Assemblies*, Vol. III, edited by F. Jurnak & A. Mc Pherson, pp. 1–71. New York: John Wiley & Sons.

Laskowski, R. A., MacArthur, M. W., Moss, D. S. & Thornton, J. M. (1993). *J. Appl. Cryst.* **26**, 283–291.

Li, R., Sirawaraporn, R., Chitnumsub, P., Sirawaraporn, W., Wooden, J., Athappilly, F., Turley, S. & Hol, W. G. J. (2000). *J. Mol. Biol.* **295**, 307–323.

Lundgren, B. (1994). *Dan. Med. Bull.* **41**, 306–318.

Luft, J. R., Rak, D. M. & DeTitta, G. T. (1999*a*). *J. Cryst. Growth*, **196**, 450–455.

Luft, J. R., Rak, D. M. & DeTitta, G. T. (1999*b*). *J. Cryst. Growth*, **196**, 447–449.

Luft, B. J. & Remington, J. S. (1992). *Clin. Infect. Dis.* **15**, 211–222.

Matthews, D. A., Bolin, J. T., Burridge, J. M., Filman, D. J., Volz, K. W., Kaufman, B. T., Beddell, C. R., Champness, J. N., Stammers, D. K. & Kraut, J. (1985). *J. Biol. Chem.* **260**, 381–391.

Otwinowski, Z. & Minor, W. (1997). *Methods Enzymol.* **276**, 307–326.

Piper, J. R., Johnson, C. A., Krauth, C. A., Carter, R. L., Hosner, C. A., Queener, S. F., Borotz, S. E. & Pfefferkorn, E. R. (1996). *J. Med. Chem.* **39**, 1271–1280.

Queener, S. F. (1991). *J. Protozool.* **38**, S154–S157.

Queener, S. F. (1995). *J. Med. Chem.* **38**, 4739–4759.

Robson, C., Meek, M. A., Grunwaldt, J-.D., Lambert, P. A., Queener, S. F., Schmidt, D. & Griffin, R. J. (1997). *J. Med. Chem.* **40**, 3040–3048.

Roos, D. S. (1993). *J. Biol. Chem.* **268**, 6269–6280.

Rosowsky, A., Cody, V., Galitsky, N., Fu, H., Papoulis, A. T. & Queener, S. F. (1999). *J. Med. Chem.* **42**, 4853–4860.

Rosowsky, A., Fu, H. & Queener, S. F. (2000). *J. Heterocycl. Chem.* **37**, 921–926.

Rosowsky, A., Papoulis, A. T., Forsch, R. A. & Queener, S. F. (1999). *J. Med. Chem.* **42**, 1007–1017.

Rosowsky, A., Papoulis, A. T. & Queener, S. F. (1997). *J. Med. Chem.* **40**, 3694–369.

Rosowsky, A., Papoulis, A. T. & Queener, S. F. (1998). *J. Med. Chem.* **41**, 913–918.

Sack, J. S. (1988). *J. Mol. Graph.* **6**, 224–225.

Sattler, F. R., Frame, P., Davis, R., Nichols, L., Shelton, B., Akil. B., Baughman, R., Highlett, C., Weiss, W., Boylen, C. T., van der Horst, C., Black, J., Powderly, W., Steigbigel, R. T., Leedom, J. M., Masur, B. & Feinberg, J. J. (1994). *Infect. Dis.* **170**, 165–172.

Sawaya, M. R. & Kraut, J. (1997). *Biochemistry*, **36**, 586–603.
Then, R. L., Hartman, P. G. & Kompis, I. (1993). *Chemistry and Biology of Pteridines and Folates*, edited by J. E. Ayling, M. G. Nair & C. M. Baugh, pp. 533–537. New York: Plenum Press.
Wang, Y., Bruenn, J. A., Queener, S. F. & Cody, V. (2001). *Antimicrob. Agents Chemother.* **45**, 2517–2523.